Environmental Science and Ecotechnology 22 (2024) 100470

Contents lists available at ScienceDirect

Environmental Science and Ecotechnology

journal homepage: www.journals.elsevier.com/environmental-science-and-ecotechnology/

Original Research

Stability of sedimentary organic matter: Insights from molecular and redox analyses

Qi Li [a, b], Chao Zhang [b], Baoqing Shan [a, b, *]

[a] State Key Laboratory of Environmental Aquatic Chemistry, Research Center for Eco-Environmental Sciences, Chinese Academy of Sciences, Beijing, 100085, China
[b] University of Chinese Academy of Sciences, Beijing, 100049, China

ARTICLE INFO

Article history:
Received 29 February 2024
Received in revised form
28 July 2024
Accepted 29 July 2024

Keywords:
Carbon stability
Redox state
FT-ICR MS
Sedimentary organic matter
Nitrogen- and sulfur-containing compounds

ABSTRACT

Sedimentary organic matter (SOM) affects the stability of the aquatic carbon pool. The degradation process of SOM is complex for its multifaceted composition. The concentration and properties of SOM affect its steady state, yet the transformation processes of SOM in lakes remain unclear. Here we show the molecular and redox perspectives of SOM stability in polluted sediments with high organic matter content and diverse vegetation. We find significant differences in carbon fractions across various sites. The origin of the organic matter, determined using excitation-emission matrix spectra, influences the consistency of organic matter composition and biochemical degradation in lacustrine sediment. We also observe that sulfur-containing substances decrease carbon chain length and reduce organic matter stability. Fourier-transform ion cyclotron resonance mass spectrometry shows that sulfur-containing substances decrease the degree of saturation and cause reduction. In contrast, nitrogen-containing compounds increase the modified aromaticity index and humin content, enhancing organic carbon complexity and stability ($p < 0.05$). These results complement the characteristics and transformations of SOM. In a broader perspective, this study contributes to laying the foundation for understanding SOM stability in the carbon cycle and its future effects.

1. Introduction

Lakes cover approximately 3% of the land surface on Earth and store an estimated 23–120 Pg of carbon (1 Pg = 10^{15} g) [1–3]. Sedimentary organic matter (SOM) is an important part of the lacustrine organic carbon cycle, accounting for approximately 70% of the organic carbon pool in global lake ecosystems [4]. In terrestrial organic matter (OM), heterotrophic microbes respire 1.2–3.3 Pg of carbon annually [5,6]. Sedimentary organic matter is a complex mixture of polymers and the degradation products of microorganisms and plant residues [7]. Determining whether OM is derived from plants or microbes is difficult [8,9]. The degradation of OM is characterized by the intrinsic stability hypothesis, in which the biologically recalcitrant fraction is limited by chemicals, and by the dilution hypothesis, in which microbial survival is limited at low concentrations and reduces the degradation rate [10,11]. Thus, the concentration and properties of OM affect its degradation, and the source of SOM can change the carbon pool.

Organic matter can be classified according to its chemical composition (e.g., carbohydrates, lignin, proteins, and other common organic compounds) or the specific organic compounds commonly present in soil and silt (e.g., humic acid [HA], fulvic acid [FA], and humin [HM]) [12]. Traditional sequential extraction methods, three-dimensional excitation–emission matrix spectroscopy (EEMS), and nuclear magnetic resonance spectroscopy are conventionally used to identify SOM [13–17]. As an alternative, Fourier-transform ion cyclotron resonance mass spectrometry (FT-ICR MS) is a promising tool that has been used to identify more than 10,000 molecular formulae [18–20]. For example, OM with the molecular formula $C_{17}H_{21}O_8$ has been found in the deep sea [21]. Liu et al. studied the effects of nitrogen and sulfur in a lacustrine environment using FT-ICR MS [22]. They suggested that dissolved organic matter (DOM) with high nutrient concentrations is often composed of high-molecular-weight, unsaturated sulfur-rich

* Corresponding author. State Key Laboratory of Environmental Aquatic Chemistry, Research Center for Eco-Environmental Sciences, Chinese Academy of Sciences, Beijing, 100085, China.
E-mail address: bqshan@rcees.ac.cn (B. Shan).

https://doi.org/10.1016/j.ese.2024.100470

compounds and polycyclic aromatic compounds [16,22]. Thus, the transformation of OM is influenced by both internal components and the external environment. Research has shown that electron transport occurs between OM and microorganisms [23–25], and this has been used in combination with the redox situation to interpret the mechanism of OM stabilization. The redox and molecular stabilities of OM are important for SOM [26,27].

Baiyangdian Lake is a large shallow lake fed by a river system in the Hai River Basin in North China. The lake has rich vegetation, including lotus, crispus, algae, and reeds. Because of its lush vegetation and environmental conditions, the sediments in the lake contain complex OM [28]. To date, few studies have investigated the composition and transformation of OM in lake sediments.

In this study, OM fraction extraction, EEMS, and parallel factor analysis (PARAFAC), as well as FT-ICR MS and X-ray photoelectron emission spectroscopy (XPS), were used to investigate the stability of OM in lacustrine sediments from Baiyangdian Lake. The objectives of this study were (1) to identify the characteristics of OM in sediments from ten sampling sites, (2) to improve our understanding of the redox state of organic carbon and its effects on OM, and (3) to illuminate SOM transformations and the effects of diverse SOM components on such transformations. These results will improve our understanding of SOM transformations in biogeochemical cycles in shallow lakes.

2. Materials and methods

2.1. Study area and sediment processing

Baiyangdian Lake (38°44′–38°59′ N, 115°45′–116°07′ E) is a large complex shallow freshwater lake system in the Xiong'an New Area. Samples were collected from ten sites in open areas (BYD1, BYD3, BYD5, BYD7, and BYD8) and channels (BYD2, BYD4, BYD6, BYD9, and FH) throughout Baiyangdian Lake at the beginning of January 2020. The details of the sampling sites are provided in the Supplementary Materials (Table S1 and Fig. S1). Three sediment core samples were collected from each sampling site, and 5 cm of the surface sediments from each sample taken at the same location were mixed in the laboratory. The samples were freeze-dried and passed through a 100-mesh sieve before analysis. The processed samples were stored at −20 °C.

We used the traditional humus extraction method of dividing SOM into water-extracted OM, FA, HA, and humus [15]. The processing steps are described in detail in Supplementary Materials and are shown in Fig. S2 [29,30]. The content of the SOM extracts was determined using a total organic carbon analyzer (SSM-5000A TOC analyzer, Shimadzu, Kyoto, Japan). The carbon compositions of water extract (WTOC), fulvic acid (FTOC), humic acid (HTOC), and HM were measured separately.

2.2. Chemical analysis

The total carbon, total nitrogen, and total sulfur contents of the sediment samples were determined using a Vario EL cube (Elementar Analysensysteme GmbH, Langenselbold, Germany). The total phosphorus content was determined using the Mo–Sb colorimetric method with a UV-4802 ultraviolet–visible (UV–vis) spectrophotometer (UV-2700, Shimadzu, Kyoto, Japan), following a method described in Chinese standard HJ 632–2011. The OM content was determined using the loss on ignition method described in Chinese standard HJ 761–2015. The zeta potential, representing the magnitude of intermolecular attraction [27,31], was determined using a Zetasizer Nano system (Malvern Panalytical, Malvern, UK). X-ray photoelectron emission spectroscopy was performed using an ESCALAB 250Xi instrument (Thermo Fisher Scientific, Waltham, MA, USA). The details of the XPS analysis are given in the Supplementary Materials and Table S5. We used the organic pollution index to evaluate the levels of organic pollution (described in the Supplementary Materials).

2.3. Fluorescence analysis

Three-dimensional EEMS of DOM was performed using a quartz cell with a 1 cm path length and an RF-6000 instrument (Shimadzu). The components were matched using the Open Fluor database. The more components present, the worse the consistency [32]. Components with similar shapes were selected to improve consistency, and the selected components had small errors. The five components (C1–C5) are shown in Table S2 and Fig. S4 (Supplementary Materials). The relative concentration of each component was determined from the fluorescence intensity and optical indices. The fluorescence index (FI), the biological index, and the humification index were used to evaluate the origin and aromaticity of DOM [21,33]. The methods used to perform the calculations are described in the Supplementary Materials.

2.4. FT-ICR MS

Each filtered water sample (after the total organic carbon [TOC] process) was passed through a solid-phase extraction (SPE) column and then infused into the electrospray ionization unit in negative ion mode. The FT-ICR MS (Solari X, Bruker, USA) pretreatment, measurement, and calculation methods are described in detail in the Supplementary Materials. The molecular formulae (C, H, O, N, and S) and molecular weights were calculated as weighted averages by normalizing the peak intensities to the sum of the FT-ICR MS peak intensities. The Van Krevelen diagram was divided using the O/C and H/C atomic ratios into seven regions, as shown in Table S3 (Supplementary Material) [34,35]. The modified aromaticity index (AI_{mod}), double bond equivalent (DBE), and nominal oxidation state of carbon (NOSC) were also calculated [36]. The degree of unsaturation was calculated using the equation (DBE-O)/C (referred to as DBE-O/C in the text). The natural OM behaving as a labile substance for the molecular lability boundary beyond the labile (MLBL) value, the carboxyl-rich alicyclic molecule (CRAM) value [37], and the degradation index (I_{DEG}) were calculated and used with the other parameters to describe OM from a molecular perspective [38]. These values are shown in Table S4 (Supplementary Material).

2.5. Statistical analysis

Two-tailed Student's *t*-tests (95% confidence level) were performed using Origin software (OriginLab, Northampton, MA, USA) to identify statistically different values for the groups of data. The relationships between the data for the different sampling sites were identified by performing correspondence analysis, nonparametric tests, regression analysis, cluster analysis, and Pearson correlation analysis using SPSS Statistics (version 25.0 software; IBM, Armonk, NY, USA). Spearman rank correlation analysis was performed on the molecular parameters using Statistical Analysis System software (Cary, NC, USA), and plots were produced using R software (version 4.2.2) with the Venn Diagram package [39]. Heatmap plots were produced using R software (version 4.2.2) with the pheatmap (v. 1.0.12) package with mean Euclidean distances.

3. Results

3.1. Spatial variations in the carbon parameters of the sediments

The TOC content range of the sediment samples, coming from

sites with heavy organic pollution, was 37.29–103.60 mg g^{-1} (Supplementary Material Fig. S3). The TOC content in the moats and the open areas was 61.76 ± 26.59 and 77.10 ± 15.12 mg g^{-1}, respectively (Fig. 1a). In addition to the WTOC values, the other components at the sites were significantly different between the moats and the open areas. Differences in the cluster analysis results (Fig. 1b and c) showed that the higher carbon content in the southern area (sites BYD8 and BYD9) influenced these differences and that the percentage of WTOC influenced the differences in distribution at site BYD8. The points in the open areas were highly aggregated, and their components were similar (Fig. 1d). However, the points in the moats were dispersed, and there were large deviations across the different carbon fractions in the moats (Fig. 1a), which were clear indications of high variability.

Humic acid was the main component of OM and contributed to >75% of the TOC (Supplementary Material Table S6 and Fig. S3). The HM content was strongly related to open water and was the main indicator with the lowest specificity (brown shaded area in Fig. 1d). Correspondence analysis showed that the HTOC content at sites FH and BYD6 was affected by human activities. The WTOC content was farthest from the origin of the correspondence analysis plot, indicating that WTOC variability was the main cause of SOM variability. The correspondence analysis value for the WTOC content was closest to the values for the moats (sites BYD2, BYD4, and BYD6). These results showed that the water type affected the four types of carbon and that WTOC had a large impact on variability in the moats.

3.2. Characteristics of DOM components in lacustrine sediments

3.2.1. Fluorescence spectroscopy and PARAFAC

The C4 fraction accounted for a large proportion (16.29–32.34%) of SOM, while the C3 fraction accounted for the smallest proportion (0.00–23.01%) (Supplementary Material Table S7). The data of the channels were different from those of the other sites (Fig. 1e–g). The C2 fraction differed significantly in terms of both water body type and location (Fig. 1e and f). Combined parallel factor analysis with the correspondence analysis (Fig. 1g), the northern points were more concentrated in the brown-shaded area, showing that they contained similar fluorescence components. By contrast, the southern points were scattered.

The data for the sources and composition characteristics were classified into three groups (Fig. 1h). The samples in group I (five points and BYD8) had low FA (C3) content that played a role in microbial reactions (FI > 1.4), and they had low degrees of biodegradability. The samples in group II (BYD2 and BYD9) were also affected by microorganisms, but the degree of biodegradability was higher. The samples in group III (BYD6 and FH) had high humus-like

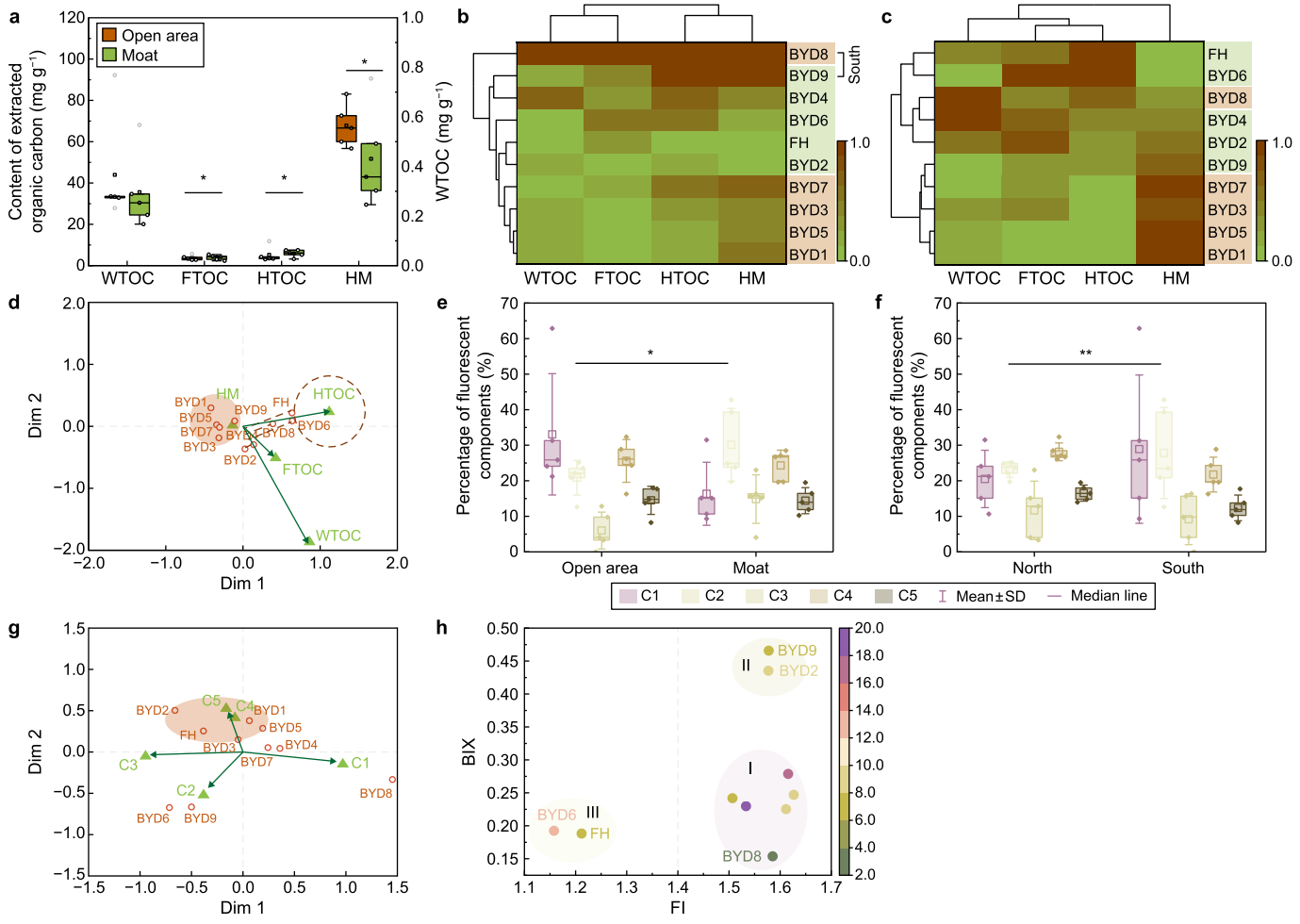

Fig. 1. Spatial differences between the types of carbon present and fluorescent components. **a**, Analysis using the significant differences of the different types of extracted carbon. **b**, Normalized cluster analysis for the carbon content normalization of multistage extraction state. **c**, Normalized cluster analysis of the carbon content ratio from multistage extraction. **d**, Correspondence analysis of the carbon types and sampling sites. **e**–**f**, Five fluorescent components separated by parallel factor analysis of the water type (**e**) and location (**f**). **g**, Correspondence analysis for three-dimensional fluorescence analysis. **h**, Fluorescence index (FI) and biological index (BIX) results used to explain regional variations in biodegradability and sources and mapping of the humification index using different colors to indicate the degree of humification.

substance content and low degrees of biodegradability, which were related to the FTOC and HTOC content. The wide variation among the moats may be related to differences in vegetation.

3.2.2. FT-ICR MS analysis of OM from SPE

The element compositions and molecular formulae determined in the preliminary analysis are shown in Table 1. There were 2732–17,031 molecular formulae (Supplementary Material Fig. S5). For the common molecular formulae (Supplementary Material Fig. S6), the compounds with the most intense peaks at most sites were $C_{17}H_{26}O_4$, $C_{18}H_{33}O_6S$, and $C_{16}H_{29}O_6S$, but the compounds with the most intense peaks for the DOM at BYD4 were $C_8H_4O_9$ and $C_{12}H_{14}O_6S$. Regarding microbial products, 20 compounds with the formula of $C_{17}H_{26}O_4$ can be derived from eight bacterial products and 12 fungal products (Supplementary Material Figs. S7 and S8, and Table S8). The molecular weights in the samples from the moats and open areas were not significantly different (Supplementary Material Fig. S10a). The components were divided into four categories: CHO-, CHON-, CHOS-, and CHONS-containing compounds. The CHO-, CHON-, and CHOS-containing compounds in the moats were highly variable (Fig. 2a). The condensed aromatic compounds, lipids, and unsaturated hydrocarbons in the moats were significantly different from those in the open areas (Fig. 2b). The standard deviation between points in the moats was large and varied significantly (Supplementary Material Table S10). Correspondence analysis and the Van Krevelen diagram at sites (Fig. 2c–e; Supplementary Material Fig. S12) showed that lipids and proteins with high molecular weights were dominant at site BYD2. Low-molecular-weight compounds, carbohydrates, and tannins were dominant at site BYD4. The DOM at site BYD6 contained condensed aromatic compounds and lignin (Supplementary Material Figs. S9 and S10). Combustion-derived polycyclic aromatic compounds were found at sites BYD9 and FH.

Correlation analyses and Venn diagrams of the cluster analysis results also showed that the compounds were more similar in the open water samples than in the channel samples (Fig. 2d; Supplementary Material Fig. S11). These results were consistent with those in Section 3.2.1 in that the DOM at site BYD2 contained fewer microbial products but could be degraded. The DOM at site BYD6 was poorly biodegradable and relatively stable. The DOM at site BYD4 contained microbial products with low biochemistry, and the molecular weight was low, which might have been caused by the content of nitrogen- and sulfur- (NS) containing compounds. The content of NS-containing compounds increased with molecular weight (Fig. 2d).

The in-depth analysis showed that the CRAM value (27.37–46.72%) increased with age (i.e., as the I_{DEG} increased from 0.24 to 0.48) and stability (i.e., as the MLBL decreased from 52.81% to 21.98%), as shown in Fig. 3a. The NOSC values in the moats (-0.10 ± 0.20), which were represented by BYD2, BYD4, and BYD6, were significantly higher than those in the open areas, and the redox values and saturation spanned a wide range (Fig. 3b and c). The DOM at BYD6 was the oldest and most biologically recalcitrant and had the most microbial regenerates, but that at BYD2 and BYD4 contained smaller amounts of regenerated products and was younger.

Unsaturated and reduced OM were more liable to degradation, and the CRAMs were mainly for unsaturated compounds (Fig. 3c; Supplementary Material Fig. S13). Non-carboxyl-rich alicyclic molecules were mainly saturated and reduced compounds. The NOSC at site BYD2 (-0.42 ± 0.52) was different from that at the other sites, and the CRAMs at this site showed few saturated and oxidized substances. Non-carboxyl-rich alicyclic molecules trended in the fourth quadrant (Fig. 3c). The number of carbon atoms also affected the NOSC. The results for most sites were similar to those for the DOM at site BYD6. The macromolecules at site BYD6 were mostly from oxidation. The longer the carbon chain of the molecule at BYD2, the more its redox state gradually converged to a weak reduction. The DOM at site BYD4 had few molecules containing over 30 carbon atoms. The number of carbon atoms and the NOSCs showed that the slope increased with the molecular weight, indicating that the carbon number increased with the redox state.

3.3. Distributions of functional groups in sediments

The functional groups on the sediment particle surfaces were identified using XPS. The main peak (52.02–69.23% of the total) for all samples was C-(H,R) (high-energy carbon spectral peak in Fig. 4). At BYD4 and BYD5, C-(O,N) was prominent (Fig. 4c). C-(OOR,OOH) and (N)-C=O,O-C-O had similar minimum angles, and the SOM at BYD2, BYD8, and BYD9 was closely related (Fig. 4a and b). The carbon valence bond and electron gains and losses showed that the functional group distribution was related to electron pair offsets, and the charges on the carbon atoms differed across samples (Fig. 4c). The surface carbon functional groups at BYD6 contained the highest proportion of C-(H,R) groups and were the most reducible. Oxidation occurred at sites BYD2, BYD4, BYD8, and BYD9. Functional groups on the surfaces of sediments at sites BYD3, BYD5, and BYD7 might have been affected by carbonate ions. The peak for the C-O bond shifted to the right (by C-H, through reduction) in the SOM at sites BYD2, BYD3, BYD4, and BYD8. A shift of the peak for the C=O double bond to the left was observed for the SOM at sites BYD5–BYD7, which could be attributed to N-containing compounds (oxidation). The full spectrum is shown in Fig. S14

Table 1
Intensity-weighted means of the molecular parameters for the samples derived from dissolved organic matter after solid-phase extracted.

Sites	Molecules number	M_w[a]	H/C_w[a]	O/C_w[a]	DBE_w[a]	MLBL (%)	CRAM (%)	$AI_{mod,w}$[a]	I_{DEG}	$NOSC_w$[a]
BYD1	7930	385.22	1.31	0.51	7.14	34.21	37.34	0.18	0.34	−0.17
BYD2	7128	416.72	1.51	0.40	6.23	52.81	32.65	0.10	0.24	−0.63
BYD3	8533	400.27	1.41	0.46	6.74	44.29	35.65	0.14	0.35	−0.37
BYD4	6128	379.95	1.35	0.57	6.26	38.02	27.37	0.18	0.28	−0.03
BYD5	8522	396.80	1.36	0.48	7.00	40.49	36.97	0.21	0.40	−0.29
BYD6	8963	408.56	1.18	0.51	8.88	21.98	46.72	0.29	0.48	−0.04
BYD7	8856	399.36	1.29	0.49	7.59	33.14	40.41	0.23	0.37	−0.19
BYD8	8664	406.70	1.27	0.50	7.85	30.01	43.94	0.21	0.48	−0.16
BYD9	8586	404.86	1.26	0.50	8.00	29.81	42.01	0.25	0.45	−0.13
FH	8458	399.69	1.43	0.44	6.52	46.57	36.64	0.14	0.43	−0.42
Average	8177	399.81	1.34	0.49	7.22	37.13	37.97	0.19	0.38	−0.24

[a] C, H, O, N, and S mean carbon, hydrogen, oxygen, nitrogen, and sulfur atoms, respectively, in the formula. Intensity-weighted means were used to calculate the molecular weight (M_w), H/C ratio, O/C ratio, double bond equivalent (DBE), modified aromaticity index (AI_{mod}), and nominal oxidation state of carbon (NOSC). Abbreviations: MLBL, natural OM behaving as a labile substance value; and CRAM, carboxyl-rich alicyclic molecules value.

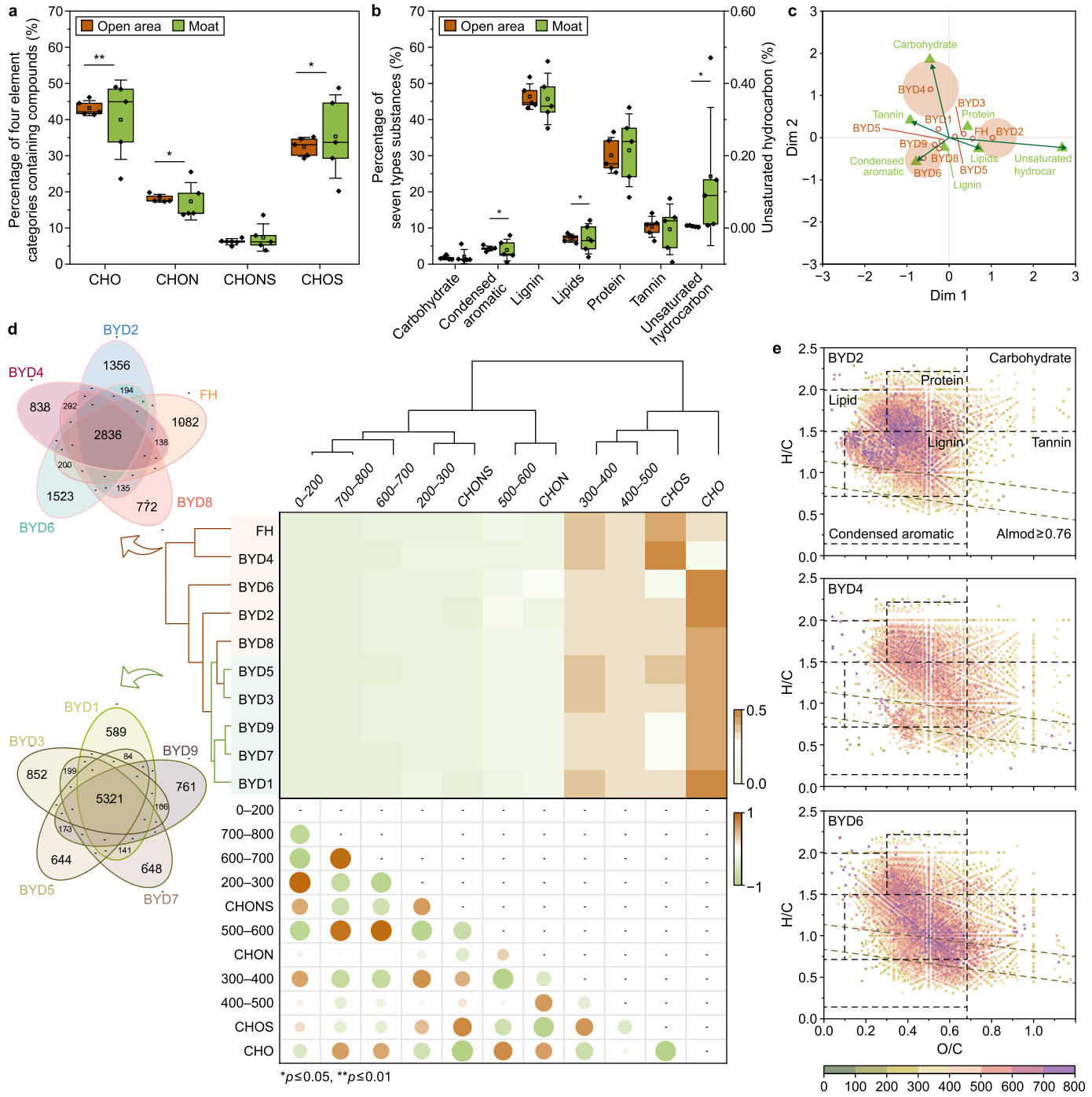

Fig. 2. Results of the Fourier-transform ion cyclotron resonance mass spectrometry analyses. **a**–**b**, The difference in the percentage of the CHO-, CHON-, and CHOS-containing compounds (**a**) and substance components composition (**b**) in open areas and moats. **c**, Correspondence analysis results indicating the differences between the compositions at the different sampling sites. **d**, Venn diagrams, clustering analysis results, and correlations between molecular weights and elemental compositions (C, H, O, N, and S). **e**, Molecular weight distributions for the different components at BYD2, BYD4, and BYD6. The colors represent the molecular weights (purple shows high molecular weight).

(Supplementary Material).

The zeta potentials were between −15.07 ± 0.34 and −20.30 ± 0.92 mV (Supplementary Material Fig. S15). The lowest zeta potential was at site BYD4, which had the strongest intermolecular attraction and a small molecular weight. The zeta potential for BYD6 indicated that its DOM was more stable than that found elsewhere, which agreed with the molecular information and XPS results. The zeta potential for BYD2 varied widely but was relatively stable.

4. Discussion

4.1. Effects of N- and S-containing substances on SOM stability

Molecules with low molecular weights were concentrated in high saturation and redox ranges (Fig. 5a and b). By contrast, those with high molecular weights were concentrated in areas with saturated and reduced OM [40]. The N and S content strongly affected molecular weight (Supplementary Material Figs. S16 and

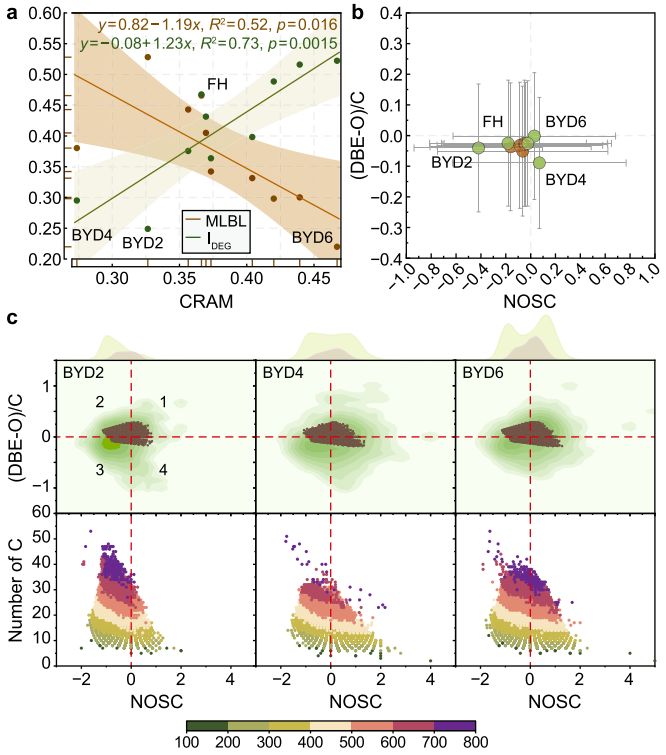

Fig. 3. Relationships between the molecule characteristics, particularly the redox state and number of carbon atoms. **a**, Linear regressions for the carboxyl-rich alicyclic molecule (CRAM) values, natural organic matter behaving as a labile substance (MLBL) value, and degradation index (I_{DEG}). **b**, The mean values of the nominal oxidation state of carbon (NOSC) and (double bond equivalent-O)/C (DBE-O/C) for molecular formulae at the different sites. **c**, Relationships between the CRAM, NOSC, and (DBE-O/C). The brown areas indicate redox and saturation conditions for carboxyl-rich alicyclic molecules. Darker green means higher density. Quadrant 1 contains unsaturated and oxidized compounds, quadrant 2 contains unsaturated and reduced compounds, quadrant 3 contains saturated and reduced compounds, and quadrant 4 contains saturated and oxidized compounds. The boundary curves were calculated using a Gaussian kernel function to estimate the density. Distributions of compounds with different molecular weights, redox states, and numbers of carbon atoms, and distributions of the numbers of carbon atoms and NOSC with kernel smoothing.

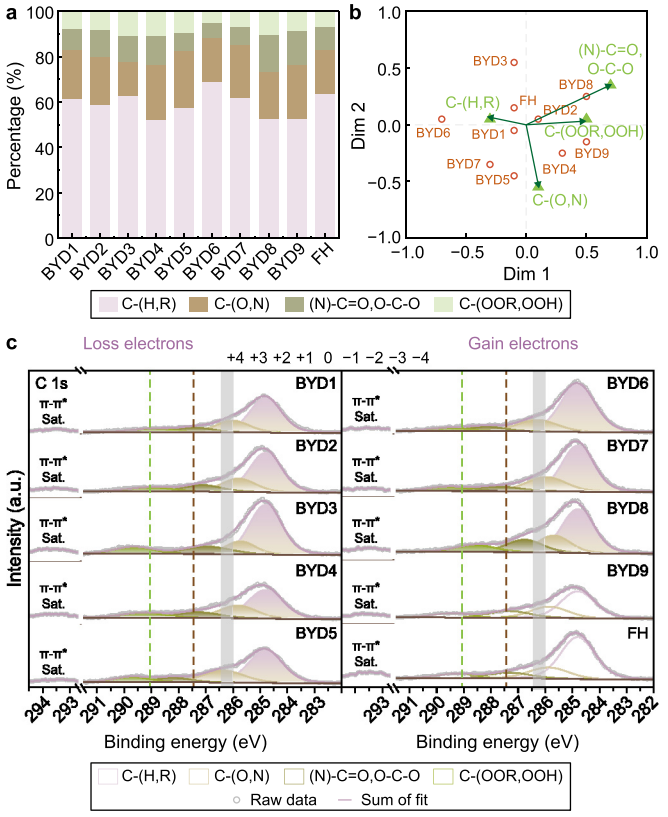

Fig. 4. X-ray photoelectron emission spectra of sediments samples from ten sites. **a**, Quantitative percentage results for C 1s peak fitting. **b**, Differences in carbon functional groups at the different sites determined by correspondence analysis. **c**, Modeled C 1s spectrum indicating the various organic carbon forms. The green dashed line represents the high valence bond of the acid radicals with carbocation at 289.4 eV, the brown dashed line represents the (N)-C=O,O-C-O type of bonds with carbocation near 287.4 eV, and the gray shadow represents the C-(N,O) type of bonds with carbocation in the range of 284.0–286.4 eV. The peak recognition information is shown in Table S5 (Supplementary Material).

S17). Nitrogen-containing compounds affected the common molecules because CHO- and CHON-containing compounds (Supplementary Material Fig. S16) were biased toward the oxidation states (NOSC >0). S-containing compounds affected the redox state for all molecular formulae because the CHOS-containing components had stronger reducibility.

Analysis of the zeta potentials and molecular formulae using Spearman correlation analysis (Fig. 5c and d) showed that 753 molecules significantly ($p < 0.05$) and positively correlated with the oxidation state (NOSC >0) and unsaturation (DBE-O/C > 0). The NOSC increased as the zeta potential increased at low intermolecular forces (mutual repulsion) and stabilities in oxidation [41]. The sediments were weakly alkaline (pH 7–7.5), meaning adsorption to form OM aggregates would create stable, large molecules containing nucleophilic functional groups through cation bridging [42,43]. The trends for the common molecules were clear (Fig. 5d), with the zeta potential being negatively correlated with the saturation and reduction state ($p < 0.05$) and with the reducing ability increasing as the unstable molecules increased. The details are provided in Supplementary Material Figs. S17 and S18.

The high total nitrogen and sulfur content results were combined because of limited microbial metabolism at low temperatures [44]. The S-containing compounds were unstable and negatively correlated with the zeta potential in their saturated and reduced states (Fig. 5e). The sulfur content was positively correlated with the WTOC. The conversion of hydrocarbons and carboxyl groups was related to the sulfur content ($p < 0.05$, Fig. 5f). The downward shift in the peak for sulfur-containing molecules indicated that sulfur-rich OM had shorter carbon chains than the other OM types (Supplementary Material Fig. S19), which explained why the sulfur content was related to the release of smaller OM and affected the stability of carbon [45,46]. The sulfur content also affected molecular consistency and was significantly negatively correlated with the number of molecules ($p < 0.05$, Supplementary Material Table S9). The nitrogen-containing compound content was positively correlated with AI_{mod} and the HM content, which indicated that nitrogen contributed to the presence of complex and stable types of organic carbon ($p < 0.05$). This was likely related to amino condensation in the Maillard reaction [47,48].

4.2. Effects of molecular components on SOM deposition and release

The analysis of the correlations between the molecules and other factors indicated that FA and HA were the most important components (Fig. 5f and g; Supplementary Material Fig. S19). Fulvic acid may mainly have been produced from HA (C4 and C5) [49] because C3 was oppositely correlated with other components

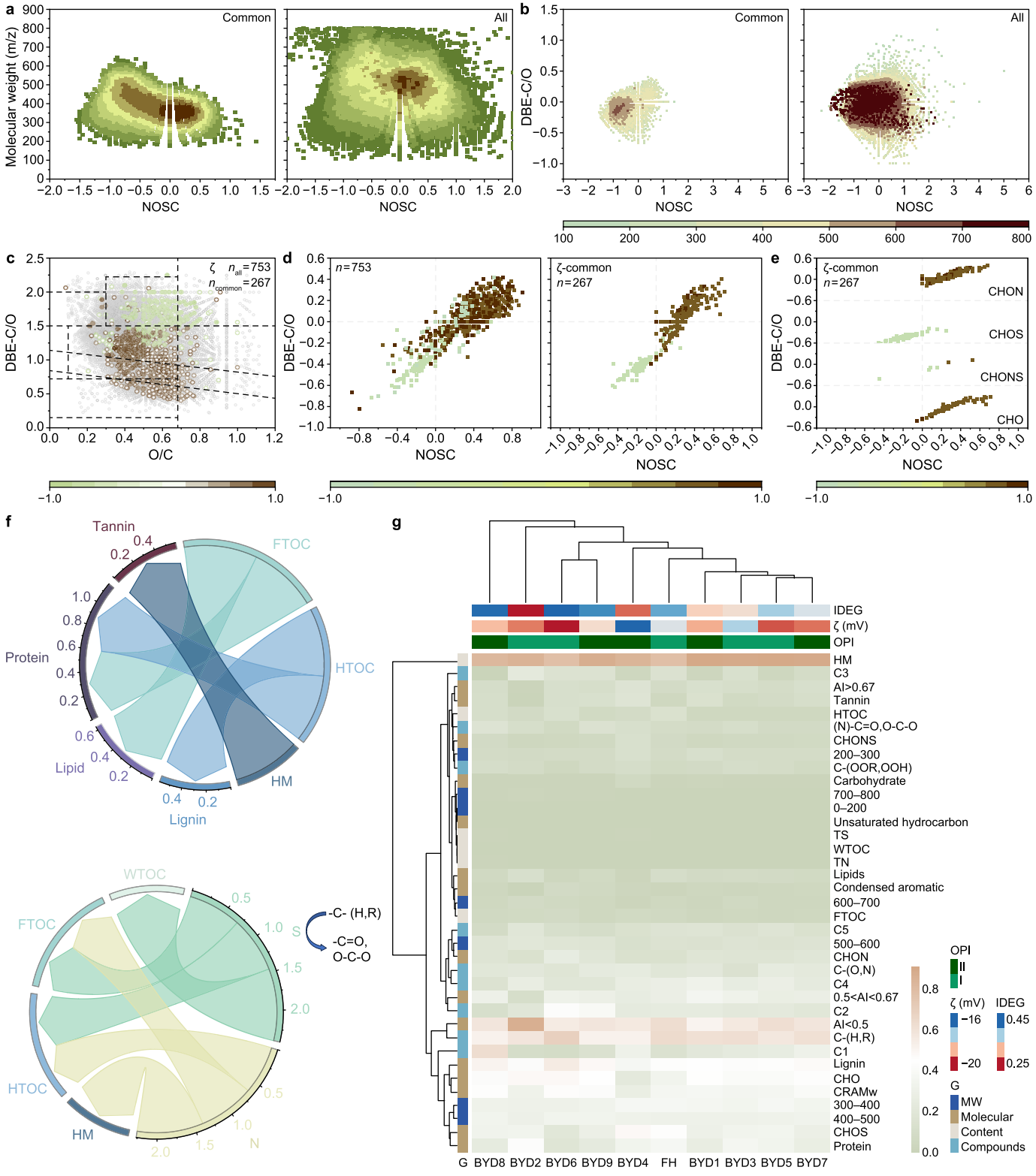

Fig. 5. Fig. 5 a, Relationships between the molecular weights and redox states of 2,732 common molecules and all the molecular formulae (classifying CHONS-containing compounds). The brown points are for higher densities and the green points are for lower densities. **b**, Relationships between the saturation and redox states of common molecules and all the molecular formulae. The colors indicate the molecular weight. **c,** Spearman correlations ($p < 0.05$) for the relationships between the zeta potentials and molecular formulae. **d,** Saturation and oxidative distribution of the 753 molecules and 267 molecules with correlations. **e,** Saturation and oxidative distribution of 267 molecules divided by elemental composition.**f**, Nitrogen- and sulfur-driven correlations between the organic matter contents and the compounds ($p < 0.05$). **g**, Heatmap plot cluster analysis results for the regions and indicators. Group G represents different variables. Green, blue, purple, and yellow represent the molecular weight, CHONS-containing components, carbon content, and the components, respectively.

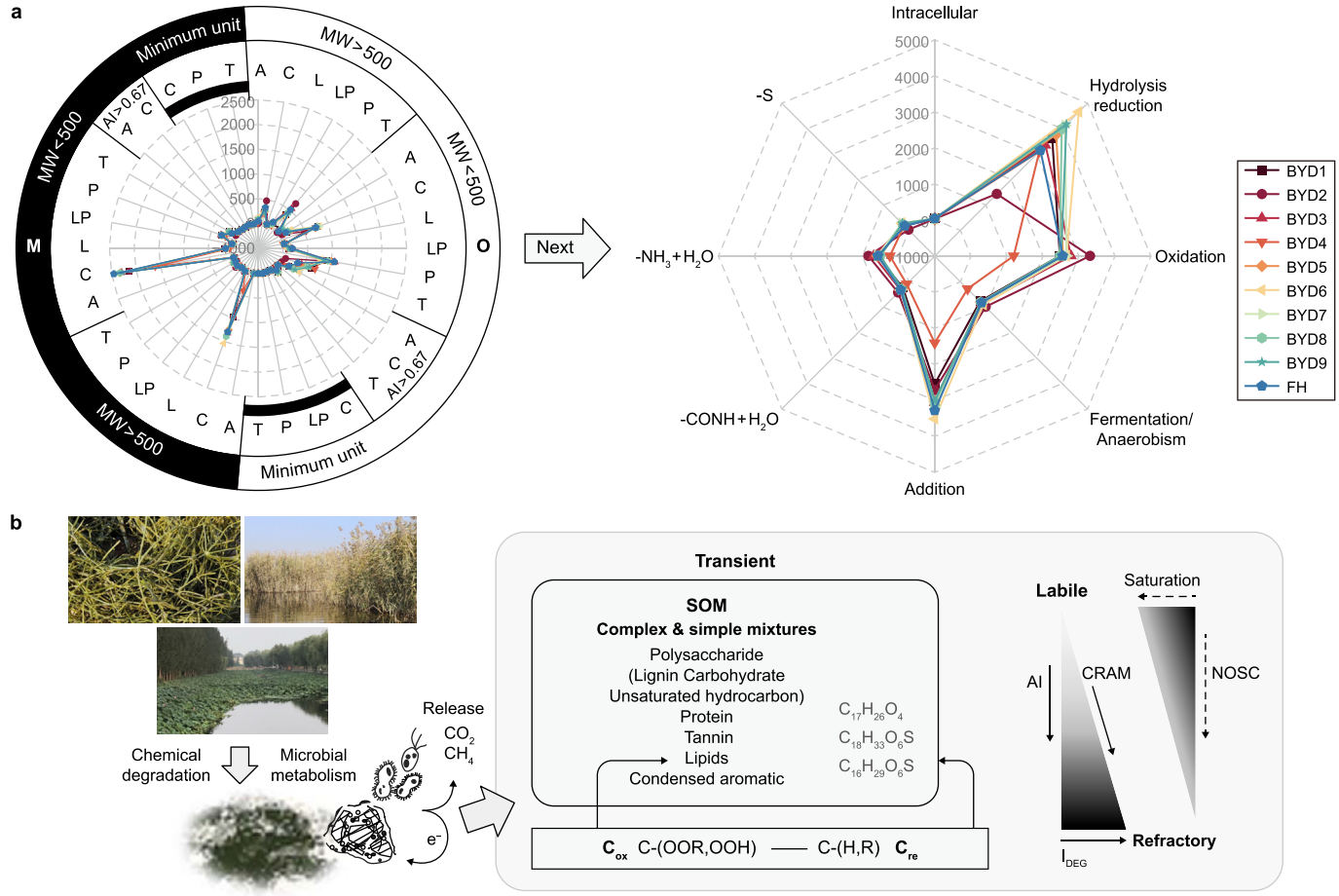

Fig. 6. **a**, Possible reactions of compounds in the sediment. The molecular formulae are divided according to the microbial product library and CRAMs into microbial products (M) and other products (O). The molecular formulae are divided into condensed aromatic compounds (A), lipids (L), complex lipids with sulfur (LP), proteins (P), polysaccharides (C, including carbohydrates, lignin, and unsaturated hydrocarbons), and tannins (T). The basic reactions and explanations are given in Table S11 (Supplementary Material). **b**, Schematic diagram of sediment decomposition.

(Supplementary Material Fig. S20). Kellerman found that C2 had a strong relationship with oxygen-rich compounds (O/C ratio >0.5) [49], which agreed with our results. Additionally, lipids and proteins were related to FTOC; lignin and condensed aromatic compounds were closely related to HTOC; and tannins and HM were related.

The zeta potential was more stable for old and intrinsically recalcitrant DOM in sediments at sites BYD6 and BYD8 than for young DOM [16]. Polymerization reactions could occur at sites BYD6 and BYD8 for different WTOCs and molecular consistency levels. C-(H,R) in the DOM at BYD6 was likely derived mostly from cellulose in reeds that were slowly degraded [50]. The limited available oxygen in the sediments would have caused lignin compounds to be preserved because most lignin compounds are mineralized by aerobic microorganisms [51]. The DOM at site BYD2 was younger than that at the other sampling sites, but intermolecular forces were still stable at site BYD2, and the macromolecules tended to be weakly reduced (Fig. 3c). Degradation may have been limited by the presence of lotus plants and microbes at BYD2 because lotus leaves, shoots, and roots contain palmitates (which are saturated), oleate and linoleate (which are monounsaturated), and macromolecular polyunsaturated acids [52,53]. Sediments at site BYD4 showed strong intermolecular attraction, which resulted in rapid degradation by algae because species such as *Potamogeton crispus* have sulfurized bacteria attached that can affect S-containing compounds in the anaerobic BYD 4 area, which is rich in sulfides [54]. These results all supported the intrinsic stability hypothesis of reactions occurring because of the compounds present rather than the concentrations of certain compounds. The degree of pollution was related to the vegetation content of the sediment, and the degradation rate was affected by the substances present.

4.3. Molecular reactions and geochemical processes in lacustrine sediments

Separating OM into reactants and products is difficult [55]. The compounds identified in the sediment samples could be regarded as products of chemical reactions (e.g., hydrolysis), microbial reactions (e.g., catalysis by enzymes), and photodegradation [9]. The molecular formulae were categorized according to the microbial product library and CRAMs into microbial products (M) and other products (O) [56] (Fig. 6a).

The proportion of microbial products at all sampling sites was 41.97–54.06%. The proportion of microbial products was highest at site BYD2, and the proportion and number of microbial products were lowest at site BYD4. The polysaccharides produced by microbial degradation were dominated by compounds with molecular weights over 500 (the boundary in Supplementary Material Fig. S10), but these only accounted for 19.92–39.22% of the total polysaccharides [44]. The proportion of macromolecular

polysaccharides was low, and the proportion of micromolecular was high at site BYD4. Microbial degradation mainly produced micromolecular polysaccharides, indicating that liquidity affected the convergence of production [54,57]. Among the other reaction products, protein products accounted for 77.70–83.68% of all the proteins present, and the proportion of micromolecular proteins was 59.60–69.90%. Site BYD2 had many amicrobic proteins but had the lowest number of tannins.

Chen [58] investigated the potential precursor–product pairs for 36 general transformation reactions of atmospheric organic compounds and found that the main reactions could be divided into demethylation, oxygenation, decarboxylation, amino reactions, nitro reactions, and sulfur reactions. In this study, the products were treated as substrates for eight types of reactions [55,56], and strong hydrolytic reduction reactions were found to occur (Fig. 6a; Supplementary Material Table S11). Multiple reactions were more likely to occur at site BYD2 than at the other sampling sites because of the complex protein sources present at this site [59].

In summary, I_{DEG}, AI_{mod}, and CRAMs gradually increased, but the NOSC and DBE-O/C tended toward zero and moved from labile to stable OM (Fig. 6b). Macromolecules (molecular weight >500) and reduced OM were found to be involved in extracellular electron migration with microorganisms. The accumulation of aromatic and aliphatic compounds and the burial of necrotic substances decreased the oxidation rate as the NOSC decreased to a weak reduction value [60]. Organic matter will always be reduced by electrons migrating between OM and microorganisms in sediment, and it is easy for electrons to be lost. This finding is consistent with a previous study [61].

5. Conclusions

This study investigated the content, components, and structures of OM in sediments from Baiyangdian Lake. We focused on the effects of the characteristics and redox abilities of the components and their possible reactions to explain the stability of SOM. The results showed that WTOC was a good indicator of SOM properties. Human disturbances and the types of water bodies were the main factors that affected variations in the extracted carbon content, OM components, and OM structures, particularly in the channels. Sulfur-containing substances decreased the carbon chain length and made OM unstable in terms of unsaturation and reduction and readily released. Nitrogen-containing compounds contributed to increased aromatization and changed OM in the oxidation state. The enhanced stability of the carbon pool is generally accompanied by increased aging processes and microbial products in SOM, with notable influences from nitrogen and sulfur. Further studies should delve deeper into the impact of sulfur. Overall, our findings provide significant insights into the stability of the carbon pool in sedimentary environments, contributing to a deeper understanding of SOM stability.

Data availability statement

The FT-ICR MS data can be requested from the author.

CRediT authorship contribution statement

Qi Li: Writing - Review & Editing, Writing - Original Draft, Visualization, Software, Methodology, Formal Analysis. **Chao Zhang:** Methodology, Formal Analysis, Data Curation, Conceptualization. **Baoqing Shan:** Resources, Methodology, Formal Analysis.

Declaration of competing interest

The authors declare that they have no known competing financial interests or personal relationships that could have appeared to influence the work reported in this paper.

Acknowledgements

We thank the staff at the State Key Laboratory Environmental Aquatic Chemistry Laboratory for sample collection and processing. We thank Yang Liu, Feifei Li, and Dong Cao (State Key Laboratory of Environmental Chemistry and Ecotoxicology) for assistance with the FT-ICR MS data. This study was funded by the National Key Research and Development Program of China (Grant No. 2022YFC3204003), the Baseline Investigation and Comprehensive Management of Ecological Environment in Baiyangdian Lake (Grant No. 20200494), the National Natural Science Foundation of China (Grant No. 41907267), and the Environmental Governance and Ecological Restoration Technical Consulting Service of Baiyangdian Lake (2022–2023; Grant No. RCEES-HX-JSFW2022000162). We thank Gareth Thomas, Ph.D., and Gabrielle David, Ph.D., from Liwen Bianji (Edanz) (https://www.liwenbianji.cn) for editing the language of a draft of this manuscript.

Appendix A. Supplementary data

Supplementary data to this article can be found online at https://doi.org/10.1016/j.ese.2024.100470.

References

[1] M. Wang, et al., Carbon accumulation and sequestration of lakes in China during the Holocene, Glob. Change Biol. 21 (2015) 4436–4448.
[2] L.A. Molot, P.J. Dillon, Storage of terrestrial carbon in boreal lake sediments and evasion to the atmosphere, Glob. Biogeochem. Cycles 10 (1996) 483–492.
[3] X. Dong, N.J. Anderson, X. Yang, X. Chen, J. Shen, Carbon burial by shallow lakes on the Yangtze floodplain and its relevance to regional carbon sequestration, Glob. Change Biol. 18 (2012) 2205–2217.
[4] Y. Du, et al., Human activity coupled with climate change strengthens the role of lakes as an active pipe of dissolved organic matter, Earth's Future 11 (2023) e2022EF003412.
[5] A.J. Tanentzap, J.A. Fonvielle, Chemodiversity in freshwater health, Science 383 (2024) 1412–1414.
[6] L.A. Kaplan, R.M. Cory, Dissolved organic matter in stream ecosystems: forms, functions, and fluxes of watershed tea, Stream Ecosyst. Chang, Environ. Times (2016) 241–320.
[7] B.P. Kelleher, A.J. Simpson, Humic substances in soils: are they really chemically distinct, Environ. Sci. Technol. 40 (2006) 4605–4611.
[8] V.N. Roth, et al., Persistence of dissolved organic matter explained by molecular changes during its passage through soil, Nat. Geosci. 12 (2019) 755–761.
[9] E.D. Whalen, et al., Clarifying the evidence for microbial- and plant-derived soil organic matter, and the path toward a more quantitative understanding, Glob. Change Biol. 28 (2022) 7167–7185.
[10] T. Dittmar, Reasons behind the long-term stability of dissolved organic matter. Biogeochemistry of Marine Dissolved Organic Matter, 2015, pp. 369–388.
[11] A. Mentges, C. Feenders, C. Deutsch, B. Blasius, T. Dittmar, Long-term stability of marine dissolved organic carbon emerges from a neutral network of compounds and microbes, Sci. Rep. 9 (2019) 17780.
[12] B. Berg, C. McClaugherty, Plant Litter: Decomposition, Humus Formation, Carbon Sequestration, Springer Berlin Heidelberg, Berlin, Heidelberg, 2014.
[13] J.W. Parsons, Humus chemistry—genesis, composition, reactions, Soil Sci. 135 (1983) 129–130.
[14] I.V. Perminova, N. Yu Grechishcheva, V.S. Petrosyan, Relationships between structure and binding affinity of humic substances for polycyclic aromatic hydrocarbons: relevance of molecular descriptors, Environ. Sci. Technol. 33 (1999).
[15] S. Bagherifam, T.C. Brown, S. Bagherifam, A. Baglieri, Sequential extraction of labile and recalcitrant fractions of soil organic matter: a case study focusing on antimony (Sb) in humic acids, fulvic acids and humin fractions of long-term aged contaminated soils, Environ. Pollut. 327 (2023) 121610.
[16] T. Dittmar, et al., Enigmatic persistence of dissolved organic matter in the ocean, Nat. Rev. Earth Environ. 2 (2021) 570–583.
[17] A. Stubbins, J.F. Lapierre, M. Berggren, Y.T. Prairie, T. Dittmar, P.A. Del Giorgio, What's in an EEM? Molecular signatures associated with dissolved organic

fluorescence in Boreal Canada, Environ. Sci. Technol. 48 (2014) 10598–10606.
[18] D.M. Nisson, et al., Radiolytically reworked Archean organic matter in a habitable deep ancient high-temperature brine, Nat. Commun. 14 (2023) 6163.
[19] J. He, et al., Responses of dissolved organic matter (DOM) characteristics in eutrophic lake to water diversion from external watershed, Environ. Pollut. 312 (2022) 119992.
[20] M. Zark, T. Dittmar, Universal molecular structures in natural dissolved organic matter, Nat. Commun. 9 (2018) 3178.
[21] X. Chen, et al., Niche differentiation of microbial community shapes vertical distribution of recalcitrant dissolved organic matter in deep-sea sediments, Environ. Int. 178 (2023) 108080.
[22] S. Liu, et al., Linking the molecular composition of autochthonous dissolved organic matter to source identification for freshwater lake ecosystems by combination of optical spectroscopy and FT-ICR-MS analysis, Sci. Total Environ. 703 (2020) 134764.
[23] Y. Bai, T. Sun, L.T. Angenent, S.B. Haderlein, A. Kappler, Electron hopping enables rapid electron transfer between quinone-/hydroquinone-containing organic molecules in microbial iron (III) mineral reduction, Environ. Sci. Technol. 54 (2020) 10646–10653.
[24] Z.-L. Chi, G.-H. Yu, A. Kappler, C.-Q. Liu, G.M. Gadd, Fungal–mineral interactions modulating intrinsic peroxidase-like activity of iron nanoparticles: implications for the biogeochemical cycles of nutrient elements and attenuation of contaminants, Environ. Sci. Technol. 56 (2022) 672–680.
[25] J. Jiang, A. Kappler, Kinetics of microbial and chemical reduction of humic substances: implications for electron shuttling, Environ. Sci. Technol. 42 (2008) 3563–3569.
[26] M.R. Kurek, et al., High voltage: the molecular properties of redox-active dissolved organic matter in northern high-latitude lakes, Environ. Sci. Technol. 57 (2023) 8617–8627.
[27] X.-Y. Liu, W. Chen, C. Qian, H.-Q. Yu, Interaction between dissolved organic matter and long-Chain ionic liquids: a microstructural and spectroscopic correlation study, Environ. Sci. Technol. 51 (2017) 4812–4820.
[28] T. Zhang, et al., Spatial and temporal dynamic response of abundant and rare aerobic denitrifying bacteria to dissolved organic matter in natural water: a case study of Lake Baiyang, China, Environ. Res. 224 (2023) 115524.
[29] G.L. Amy, M.R. Collins, C.J. Kuo, P.H. King, Comparing gel permeation chromatography and ultrafiltration for the molecular weight characterization of aquatic organic matter, J. AWWA (Am. Water Works Assoc.) 79 (1987) 43–49.
[30] E.M. Thurman, R.L. Malcolm, Preparative isolation of aquatic humic substances, Environ. Sci. Technol. 15 (1981) 463–466.
[31] M.C. Smith, R.M. Crist, J.D. Clogston, S.E. McNeil, Zeta potential: a case study of cationic, anionic, and neutral liposomes, Anal. Bioanal. Chem. 409 (2017) 5779–5787.
[32] C.A. Stedmon, R. Bro, Characterizing dissolved organic matter fluorescence with parallel factor analysis: a tutorial: fluorescence-PARAFAC analysis of DOM, Limnol Oceanogr. Methods 6 (2008) 572–579.
[33] T. Ohno, Fluorescence inner-filtering correction for determining the humification index of dissolved organic matter, Environ. Sci. Technol. 36 (2002) 742–746.
[34] K. Sun, et al., Application of hydrochar altered soil microbial community composition and the molecular structure of native soil organic carbon in a paddy soil, Environ. Sci. Technol. 54 (2020) 2715–2725.
[35] Y. Zhang, K. Yang, H. Chen, Y. Dong, W. Li, Origin, composition, and accumulation of dissolved organic matter in a hypersaline lake of the Qinghai-Tibet Plateau, Sci. Total Environ. 868 (2023) 161612.
[36] Y. Ding, et al., Chemodiversity of soil dissolved organic matter, Environ. Sci. Technol. 54 (2020) 6174–6184.
[37] N. Hertkorn, et al., Characterization of a major refractory component of marine dissolved organic matter, Geochim. Cosmochim. Acta. 70 (2006) 2990–3010.
[38] T. Riedel, H. Biester, T. Dittmar, Molecular fractionation of dissolved Organic matter with metal salts, Environ. Sci. Technol. 46 (2012) 4419–4426.
[39] H. Chen, P.C. Boutros, Venn Diagram: a package for the generation of highly-customizable Venn and Euler diagrams in R, BMC Bioinf. 12 (2011) 35.
[40] D. Leyva, M. Usman Tariq, R. Jaffé, F. Saeed, F. Fernandez-Lima, Description of dissolved organic matter transformational networks at the molecular level, Environ. Sci. Technol. 57 (2023) 2672–2681.
[41] H. Wang, et al., Colloidal stability of Fe_3O_4 magnetic nanoparticles differentially impacted by dissolved organic matter and cations in synthetic and naturally-occurred environmental waters, Environ. Pollut. 241 (2018) 912–921.
[42] R.M. Boiteau, et al., Calcareous organic matter coatings sequester siderophores in alkaline soils, Sci. Total Environ. 724 (2020) 138250.
[43] Y. Han, Pollution Characteristics and Source Sink Process in Sediments of Baiyang Lake (Thesis for Master Degree), Hebei University (Chinese), 2021.
[44] C. Gong, et al., Enhanced chemodiversity, distinctive molecular signature and diurnal dynamics of dissolved organic matter in streams of two headwater catchments, Southeastern China, Water Res 211 (2022) 118052.
[45] P. Chauhan, S. Mahajan, D. Enders, Organocatalytic carbon-sulfur bond-forming reactions, Chem. Rev. 114 (2014) 8807–8864.
[46] G. Muyzer, A.J.M. Stams, The ecology and biotechnology of sulphate-reducing bacteria, Nat. Rev. Microbiol. 6 (2008) 441–454.
[47] D. Hemmler, C. Roullier-Gall, J.W. Marshall, M. Rychlik, A.J. Taylor, P. Schmitt-Kopplin, Insights into the chemistry of non-enzymatic browning reactions in different ribose-amino acid model systems, Sci. Rep. 8 (2018) 16879.
[48] O.W. Moore, et al., Long-term organic carbon preservation enhanced by iron and manganese, Nature 621 (2023) 312–317.
[49] A.M. Kellerman, D.N. Kothawala, T. Dittmar, L.J. Tranvik, Persistence of dissolved organic matter in lakes related to its molecular characteristics, Nat. Geosci. 8 (2015) 454–457.
[50] S. Liu, X. Ge, L.N. Liew, Z. Liu, Y. Li, Effect of urea addition on giant reed ensilage and subsequent methane production by anaerobic digestion, Bioresour. Technol. 192 (2015) 682–688.
[51] P.J. Van Soest, Nutritional Ecology of the Ruminant, Cornell University Press, 1994.
[52] Y. Bi, G. Yang, H. Li, G. Zhang, Z. Guo, Characterization of thechemical composition of lotus plumule oil, J. Agric. Food Chem. 54 (2006) 7672–7677.
[53] Y. Nakamura, Y. Li-Beisson (Eds.), Lipids in Plant and Algae Development, Subcellular Biochemistry, vol. 86, Springer International Publishing, Cham, 2016.
[54] S. Liu, et al., Molecular-level composition of dissolved organic matter in distinct trophic states in Chinese lakes: implications for eutrophic lake management and the global carbon cycle, Water Res. 217 (2022) 118438.
[55] E.D. Schroeder, T.M. Young, Aquatic chemistry, in: third ed.Eos Trans. Am. Geophys. Union, vol. 77, 1996, 284–284.
[56] A. Hu, L. Li, Y. Huang, Q.-L. Fu, D. Wang, W. Zhang, Photochemical transformation mechanisms of dissolved organic matters (DOM) derived from different bio-stabilization sludge, Environ. Int. 169 (2022) 107534.
[57] N.W. Sokol, M.A. Bradford, Microbial formation of stable soil carbon is more efficient from belowground than aboveground input, Nat. Geosci. 12 (2019) 46–53.
[58] S. Chen, et al., Source and formation process impact the chemodiversity of rainwater dissolved organic matter along the Yangtze River Basin in summer, Water Res. 211 (2022) 118024.
[59] X. Guan, et al., Natural polyphenol tannin-immobilized composites: rational design and versatile applications, J. Mater. Chem. B 11 (2023) 4619–4660.
[60] A. Gunina, Y. Kuzyakov, From energy to (soil organic) matter, Glob. Change Biol. 28 (2022) 2169–2182.
[61] S. Bertilsson, J.B. Jones, Supply of Dissolved Organic Matter to Aquatic Ecosystems, Autochthonous Sources, 2003.